RESEARCH ARTICLE

Antitumor Activity Associated with Prolonged Persistence of Adoptively Transferred NY-ESO-1^{c259}T Cells in Synovial Sarcoma

Sandra P. D'Angelo[1], Luca Melchiori[2], Melinda S. Merchant[3], Donna Bernstein[3], John Glod[3], Rosandra Kaplan[3], Stephan Grupp[4], William D. Tap[1], Karen Chagin[2], Gwendolyn K. Binder[2], Samik Basu[2], Daniel E. Lowther[2], Ruoxi Wang[2], Natalie Bath[2], Alex Tipping[2], Gareth Betts[2], Indu Ramachandran[2], Jean-Marc Navenot[2], Hua Zhang[3], Daniel K. Wells[5], Erin Van Winkle[2], Gabor Kari[2], Trupti Trivedi[2], Tom Holdich[2], Lini Pandite[2], Rafael Amado[2], and Crystal L. Mackall[3,5,6]

ABSTRACT We evaluated the safety and activity of autologous T cells expressing NY-ESO-1^{c259}, an affinity-enhanced T-cell receptor (TCR) recognizing an HLA-A2–restricted NY-ESO-1/LAGE1a–derived peptide, in patients with metastatic synovial sarcoma (NY-ESO-1^{c259}T cells). Confirmed antitumor responses occurred in 50% of patients (6/12) and were characterized by tumor shrinkage over several months. Circulating NY-ESO-1^{c259}T cells were present postinfusion in all patients and persisted for at least 6 months in all responders. Most of the infused NY-ESO-1^{c259}T cells exhibited an effector memory phenotype following *ex vivo* expansion, but the persisting pools comprised largely central memory and stem-cell memory subsets, which remained polyfunctional and showed no evidence of T-cell exhaustion despite persistent tumor burdens. Next-generation sequencing of endogenous TCRs in CD8$^+$ NY-ESO-1^{c259}T cells revealed clonal diversity without contraction over time. These data suggest that regenerative pools of NY-ESO-1^{c259}T cells produced a continuing supply of effector cells to mediate sustained, clinically meaningful antitumor effects.

SIGNIFICANCE: Metastatic synovial sarcoma is incurable with standard therapy. We employed engineered T cells targeting NY-ESO-1, and the data suggest that robust, self-regenerating pools of CD8$^+$ NY-ESO-1^{c259}T cells produce a continuing supply of effector cells over several months that mediate clinically meaningful antitumor effects despite prolonged exposure to antigen. *Cancer Discov; 8(8); 944–57. ©2018 AACR.*

See related commentary by Keung and Tawbi, p. 914.

INTRODUCTION

Synovial sarcoma represents approximately 5% of all soft-tissue sarcomas and is characterized by a translocation between SYT on the X chromosome and SSX1, SSX2, SSX4 on chromosome 18 (1). Seventy percent of synovial sarcoma diagnoses occur in patients under 40 years old. Standard therapy for localized disease includes surgical resection with or without radiotherapy, and there is no clearly established role for neoadjuvant or adjuvant chemotherapy (1). In patients with metastatic disease, cytotoxic chemotherapy with agents such as anthracyclines, ifosfamide, trabectedin, or pazopanib can stabilize disease or induce regression in some patients, but the expected 5-year overall survival (OS) is dismal, highlighting the need for more effective therapies (1).

T cells can mediate potent and long-lived antitumor effects, as illustrated by the prolonged duration of benefit following ipilimumab in melanoma (2) and PD-1/PD-L1 blockade in an increasing number of tumor histologies (3–7). However, response to checkpoint blockade varies widely, and checkpoint-responsive histologies typically demonstrate high levels of immunogenicity as measured by nonsynonymous somatic mutation (nSSM) burden (8–11), T-cell infiltration, or PD-L1 expression (7). Like other translocation-driven cancers, synovial sarcoma demonstrates a relative paucity of nSSMs (12), which likely explains its unresponsiveness to checkpoint blockade (13). In contrast, 70% to 80% of synovial sarcomas express NY-ESO-1 (14–16), an immunogenic cancer testis antigen that has been targeted using vaccines (17–21) and adoptive transfer of T cells engineered to express NY-ESO-1^{c259}, an affinity-enhanced T-cell receptor (TCR) targeting NY-ESO-1/LAGE1a (22–25).

Previous experience with adoptively transferred NY-ESO-1^{c259}T cells plus high-dose IL2 reported clinical responses in 11 of 18 patients (61%) with refractory synovial sarcoma (22, 23). In those studies, a correlation between response and expansion of the adoptively transferred cells as measured at 30 days was not observed, and persistence of NY-ESO-1^{c259}T cells beyond 30 days was not reported. Here, we report clinical outcomes along with the characteristics of persistent transduced cells from the initial cohort in a pilot trial assessing NY-ESO-1^{c259}T cells (SPEAR T cells) in patients with advanced synovial sarcoma.

RESULTS

Patient Characteristics and Treatment Regimen

The study protocol specified that this cohort contain 10 evaluable patients. We screened 120 patients with synovial sarcoma for HLA-A*02 and NY-ESO-1 expression. Fifteen patients (median age, 29 years; range, 18–51 years) with recurrent and/or metastatic synovial sarcoma were enrolled and underwent leukapheresis (Supplementary Fig. S1). Of the 15 enrolled patients, 14 were HLA-A*02-01 and 1 was HLA-A*02-06

[1]Memorial Sloan Kettering Cancer Center and Weill Cornell Medical College, New York, New York. [2]Adaptimmune, Oxford, United Kingdom, and Philadelphia, Pennsylvania. [3]Pediatric Oncology Branch, NCI, Bethesda, Maryland. [4]Children's Hospital of Philadelphia, Philadelphia, Pennsylvania. [5]Parker Institute for Cancer Immunotherapy, San Francisco, California. [6]Stanford University, Stanford, California.

Note: Supplementary data for this article are available at Cancer Discovery Online (http://cancerdiscovery.aacrjournals.org/).

S.P. D'Angelo and L. Melchiori contributed equally to this article.

Corresponding Author: Sandra P. D'Angelo, Memorial Sloan Kettering Cancer Center and Weill Cornell Medical College, 300 East 66th Street, New York, NY 10065. Phone: 646-888-4159; Fax: 646-888-4252; E-mail: dangelos@mskcc.org

doi: 10.1158/2159-8290.CD-17-1417

Table 1. Characteristics of treated patients and results[a]

Patient	Age at screening	Gender	Prior chemotherapy regimens (# lines of therapy: names of agents)	Transduced cell dose ($\times 10^9$)	Best overall response	Duration of response (weeks)	Peak cell expansion (vector copies/mg DNA)
200	41	M	3: doxorubicin + ifosfamide, ifosfamide, docetaxel + gemcitabine	14.355	SD	.	43,181
201	32	F	2: ifosfamide + vincristine + doxorubicin, ifosfamide	8.328	CR	34	104,115
202	19	F	2: doxorubicin + ifosfamide, trabectedin	6.64	PR	34	110,610
204	24	F	1: doxorubicin, ifosfamide	3.79	PR	16	77,401
205	19	F	1: doxorubicin, ifosfamide	3.4	PR	13	192,445
206	29	M	2: doxorubicin + ifosfamide, ifosfamide	0.451	SD	.	11,265
207	27	M	4: doxorubicin + ifosfamide, Adriamycin + ifosfamide, etoposide + ifosfamide, gemcitabine or docetaxel ± Morab (clinical trial)	2.67	SD	.	19,939
208	32	M	3: doxorubicin, ifosfamide, docetaxel + gemcitabine	2.23	PR	72	108,233
209	32	F	4: cyclophosphamide, Adriamycin + ifosfamide, ifosfamide, phase I dendritic cell therapy	6.45	PR	28	76,185
230	18	F	1: doxorubicin, ifosfamide	7.863	SD	.	41,263
261	38	M	4: docetaxel + gemcitabine, pazopanib, MEK inhibitor, ifosfamide	0.721	SD	.	17,655
263	51	M	1: doxorubicin	2.511	SD	.	119,883

[a]Data cutoff March 30, 2017.

Abbreviations: F, female; M, male; SD, stable disease.

positive. The majority of patients had received at least 2 lines of prior chemotherapy. Three patients had rapid disease progression following enrollment and did not receive treatment. The remaining 12 patients received a lymphodepleting preparative regimen, comprised of fludarabine 30 mg/m^2 on days −4 to −1 and cyclophosphamide 1,800 mg/m^2 on days −2 and −1, followed by cell infusion on day 0. Table 1 summarizes the demographics, clinical response, and cell infusion doses for these 12 patients. The median-infused NY-ESO-1^{259}T-cell dose was 3.6 $\times 10^9$ (range, 0.45–14.4 $\times 10^9$) transduced cells. Manufactured products meeting the minimum protocol-specific dose of 1 $\times 10^9$ NY-ESO-1^{259}T cells were successfully generated from 10 of 12 patients; the remaining 2 patients were infused with cell numbers below the protocol-specified dose.

NY-ESO-1^{c259}T Cells Mediate Immune Regression of Synovial Sarcoma over Several Months

Patients infused with NY-ESO-1^{c259}T cells on this trial demonstrated a median time to initial response of 6.2 weeks (range, 4–9 weeks) and a median duration of response of 30.9 weeks (range, 13–72 weeks; Table 1). The overall response rate (ORR) in this study cohort was 50%, with 1 confirmed complete response (CR) and 5 confirmed partial responses (PR; 95% Clopper–Pearson confidence interval, 0.21–0.79). The median progression-free survival (PFS) was 15 weeks (range, 8–38 weeks). One responder (patient 205) underwent surgical resection prior to progression and therefore is censored for this endpoint from the time of resection. The current estimate of the median OS is approximately 120 weeks (range, 37 weeks–undetermined value, as the upper bound has not been reached; Fig. 1A). Five patients are alive (at March 30, 2017, data cutoff), including 2 patients (patients 202, 204) who progressed following response but underwent surgical resection at the time of progression (Fig. 1B). An additional patient (patient 201) underwent surgical resection at the time of progression, but subsequently died. Therefore, the proportion censored at the time of data cutoff is 5/12 (42%), and a longer follow-up time is needed to better estimate the median OS with precision. Two patients who received a subtarget (<1 $\times 10^9$) transduced cell dose progressed within 12 weeks.

The pace of antitumor response was not compatible with antitumor effects mediated solely by chemotherapy. Maximal effects of chemotherapy are typically observed within 4 weeks of treatment; however, 7 patients experienced continued decreases in tumor burden following the 4-week evaluation

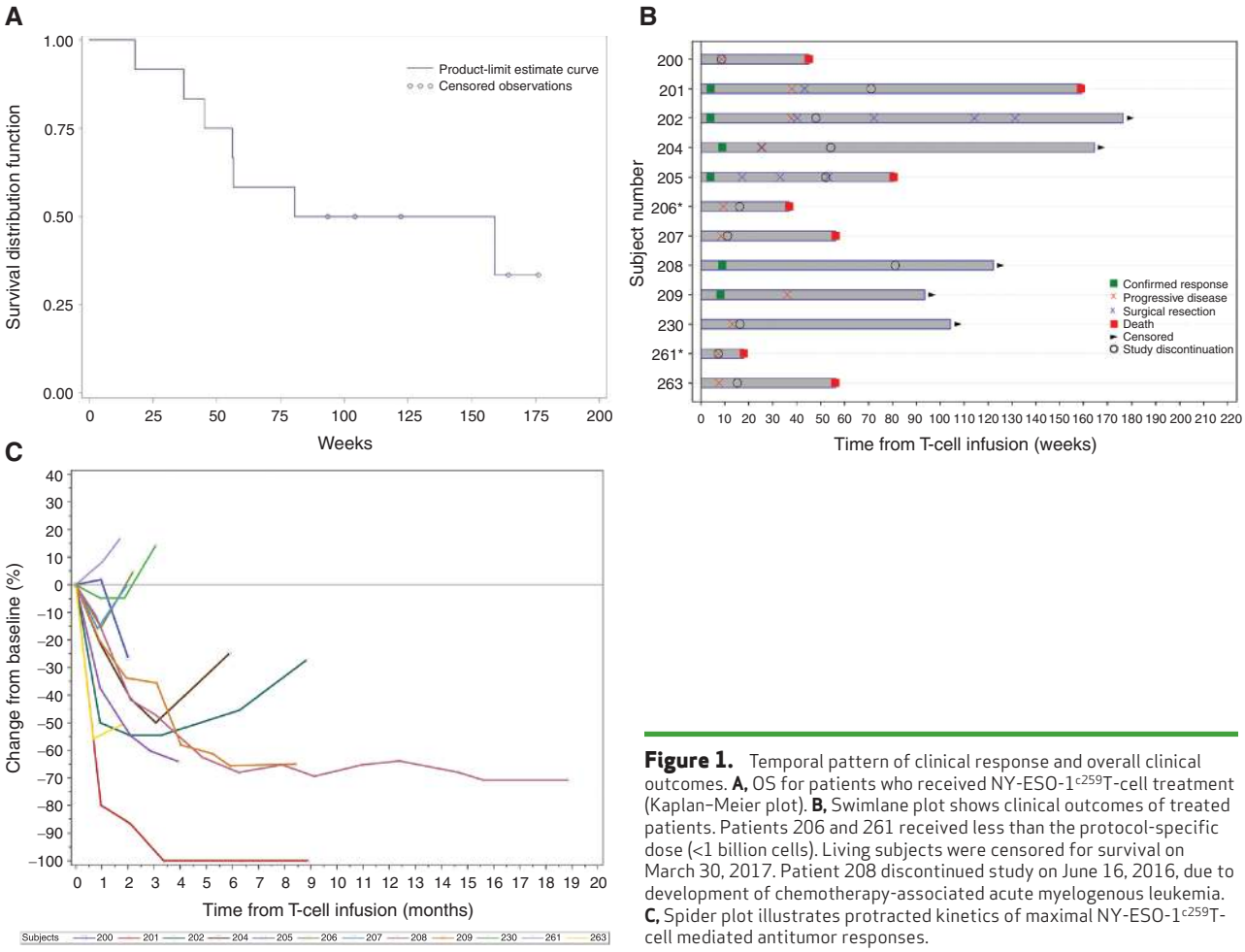

Figure 1. Temporal pattern of clinical response and overall clinical outcomes. **A,** OS for patients who received NY-ESO-1^{c259}T-cell treatment (Kaplan–Meier plot). **B,** Swimlane plot shows clinical outcomes of treated patients. Patients 206 and 261 received less than the protocol-specific dose (<1 billion cells). Living subjects were censored for survival on March 30, 2017. Patient 208 discontinued study on June 16, 2016, due to development of chemotherapy-associated acute myelogenous leukemia. **C,** Spider plot illustrates protracted kinetics of maximal NY-ESO-1^{c259}T-cell mediated antitumor responses.

point (Fig. 1C). Maximal antitumor responses occurred in 4 patients more than 3 months following cell infusion. Several features of the clinical course of patients treated on this study demonstrate that antitumor effects were immune-mediated. Patient 201 demonstrated transient radiographic worsening of miliary lung metastases within 48 hours following cell infusion associated with increased circulating C-reactive protein levels, followed by a CR lasting until 9 months postinfusion (Fig. 2A and B). We also observed direct evidence of tumor trafficking by NY-ESO-1^{c259}T cells in patient 206, who received a dose of NY-ESO-1^{c259}T cells below the protocol-specified minimum dose (Table 1), then developed signs and symptoms consistent with a delayed cytokine release syndrome (CRS) on day 56 following cell infusion. On day 60, surgical resection of an enlarging tumor mass (Fig. 2C) and drainage of pleural fluid was performed, which demonstrated NY-ESO-1^{c259}T cells within both the tumor mass and the pleural fluid (Fig. 2D).

Toxicity of NY-ESO-1^{c259}T Cells

There were no fatal serious adverse events in this treatment cohort. Adverse events ≥ grade 3 were reported in all 12 treated patients, and these were deemed treatment related in 11 patients. The most common adverse events ≥ grade 3 among the 12 treated subjects were lymphopenia (100%), leukopenia (92%), neutropenia (83%), anemia (83%), hypophosphatemia (75%), and thrombocytopenia (67%). The incidence of ≥ grade 3 febrile neutropenia was 17%. Five patients experienced CRS of grades 1 (n = 2), 2 (n = 1), and 3 (n = 2). CRS occurred within a median of 4 days (range, 0–11 days; 1 instance occurred on the day of treatment). The median duration of CRS was 10 days (range, 8–28 days). No events of seizure, cerebral edema, or encephalopathy were reported. Patients were monitored by PCR and found negative for replication-competent lentivirus. In patients in which more than 1% of the peripheral blood mononuclear cells (PBMC) were vector-positive at 6 months postinfusion (n = 4), clonality assessment was carried out to exclude insertional oncogenesis as a mechanism for persistence. All analyzed samples, collected from 6 to 21 months postinfusion, showed a high level of polyclonality of the transduced population and the absence of dominant clones.

In Vivo Expansion and Persistence of NY-ESO-1^{c259}T Cells

We used PCR to quantitate circulating NY-ESO-1^{c259} vector copies following T-cell infusion. NY-ESO-1^{c259}T cells were detectable in all patients following infusion, with peak levels measured within the first 10 days after infusion. Peak NY-ESO-1^{c259} vector copy levels (P_{max}) were statistically

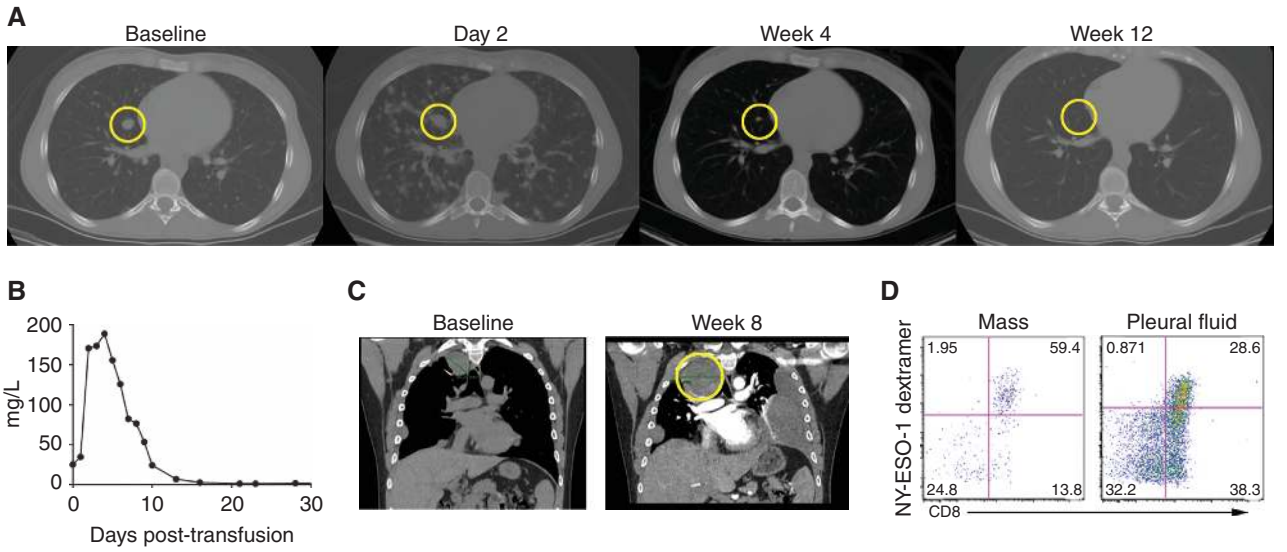

Figure 2. Transient radiographic progression and tumor trafficking of NY-ESO-1^{c259}T cells. **A,** At the designated times following infusion of NY-ESO-1^{c259}T cells, miliary synovial sarcoma involving the lungs of patient 201 demonstrates radiographic progression on day 2, PR at week 4, and then CR at week 12, which persisted for 9 months. **B,** Radiographic progression on day 2 shown in **A** was associated with fever and elevated circulating C-reactive protein. **C,** Patient 206 presented with tumor enlargement, increased pleural fluid, fever, and constitutional symptoms on day 60 following NY-ESO-1^{c259}T-cell infusion. **D,** The pleural mass highlighted in yellow in **C** was resected and pleural fluid drained. NY-ESO-1^{c259}T cells identified by dextramer binding via flow cytometry were present within the tumor mass (left) and within the pleural fluid (right).

significantly higher (P = 0.0411) in responders (median, 106,174 vector copies/μg; range, 76,185–192,445) compared with nonresponders (median, 30,601 vector copies/μg; range, 11,265–119,883; Fig. 3A). Using 75,000 as a *post hoc* cutoff, 6 of 6 responders demonstrated P_{max} >75,000 vector copies/μg of DNA, and 1 of 6 nonresponders demonstrated P_{max} >75,000 vector copies/μg of DNA. Among 7 patients for whom monitoring continued beyond 200 days, circulating NY-ESO-1^{c259}TCR-expressing T cells were detected (Fig. 3B and C; Supplementary Fig. S2). The persisting cells were polyfunctional, as determined by intracellular cytokine staining (Supplementary Fig. S3). CD4$^+$ and CD8$^+$ NY-ESO-1^{c259}T cells persisting in the blood remained virtually negative for exhaustion markers such as PD-1 and LAG3 for the duration of the analysis period (Supplementary Fig. S2). Thus, NY-ESO-1^{c259}T cells expand significantly *in vivo* in responding patients and demonstrate long-term persistence and functionality (Fig. 3D) associated with clinically meaningful antitumor effects.

The Persistent NY-ESO-1^{c259}T-cell Pool Is Enriched for TSCM and TCM Subsets

We assessed the memory cell phenotype of NY-ESO-1^{c259}TCR-expressing T cells in the manufactured product and following infusion in a subset of patients. As expected, due to the *ex vivo* expansion method used, NY-ESO-1^{c259}T cells present in the manufactured product predominantly comprised effector memory (TEM; CCR7$^-$CD45RA$^-$) or effector memory RA$^+$ (TEMRA; CCR7$^-$CD45RA$^+$) cells, with lower proportions of central memory (TCM; CCR7$^+$CD45RA$^-$) or stem cell memory (TSCM; CCR7$^+$CD45RA$^+$) cells (Fig. 4A–C; Supplementary Fig. S2). Although the power to detect correlates of response is diminished due to small numbers of patients, we found no differences between manufactured products administered to responders versus nonresponders with regard to proportions of CD4 versus CD8, proportions of TEM, TEMRA, TSCM, or TCM, other cell-surface markers, or NY-ESO-1–induced cytokine production. Following adoptive transfer, we consistently observed an increase in the frequency of TSCM and TCM subsets within the circulating CD4$^+$ and CD8$^+$ NY-ESO-1^{c259}T-cell pool, which occurred within the first month and persisted for the duration of our evaluation. Whereas both the CD4$^+$ and CD8$^+$ NY-ESO-1^{c259}T-cell pool were enriched for TSCMs, the CD4$^+$ NY-ESO-1^{c259}T-cell pool was significantly enriched for the TCM subset compared with the CD8$^+$ NY-ESO-1^{c259}T cells (P = 0.044). Compiled data for the entire cohort of patients are shown in Fig. 4C.

A high proportion of NY-ESO-1^{c259}T cells persisting as long as 28 months postinfusion in patient 202 enabled functional analysis in this patient (Fig. 3C). Cells maintained robust expression of CCR7$^+$ and CD45RA$^+$ (Supplementary Fig. S4). Exposure to antigen *ex vivo* induced robust killing in the absence of exogenous cytokines (Fig. 3D), and although more differentiated effector cells were generated after killing, a significant pool of CCR7$^+$ and CD45RA$^+$ cells was maintained, suggesting self-renewal and differentiation ability. Despite persistence of circulating functional NY-ESO-1^{c259}T cells, this patient's disease relapsed, and at resection the recurrent tumor continued to stain positive for NY-ESO-1 expression (Supplementary Fig. S5). However, we observed no evidence for infiltration of the tumor by NY-ESO-1^{c259}T cells. Additional postrelapse biopsies were assessed for antigen expression, and NY-ESO-1 continued to be expressed in 5 of 6 samples tested from patient 202 and 1 of 1 sample tested from patient 209 (Supplementary Fig. S6). Although

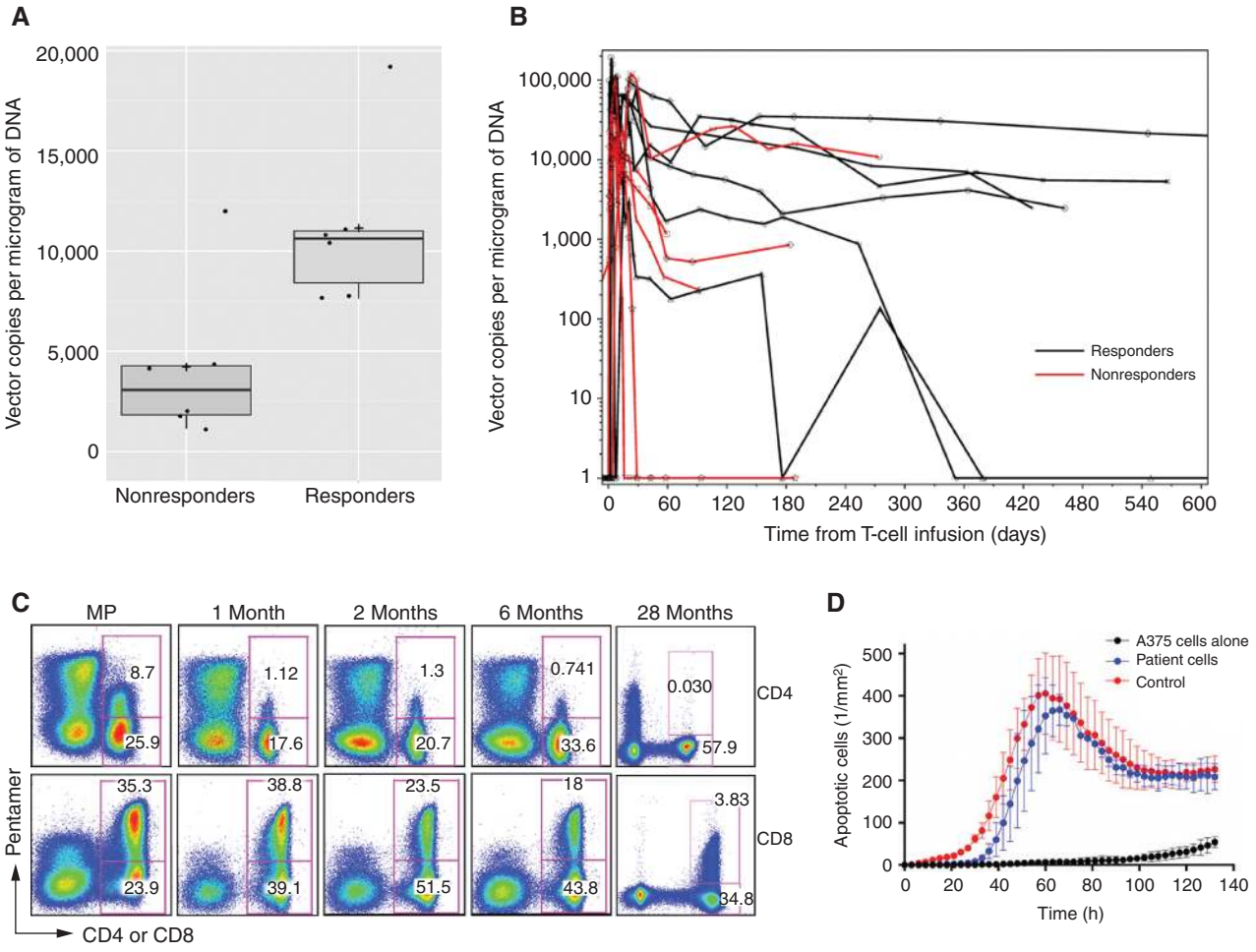

Figure 3. NY-ESO-1^{c259}T cells show increased expansion in responding patients and persist with functional capacity to kill NY-ESO-1 targets for several months. **A,** Peak vector copies/μg of DNA demonstrating T-cell expansion in nonresponders ($n = 6$) versus responders ($n = 6$). **B,** T-cell persistence in nonresponders ($n = 6$) versus responders ($n = 6$). **C,** Enumeration of CD4$^+$ (top) and CD8$^+$ (bottom) NY-ESO-1^{c259}T cells based upon binding to NY-ESO-1 pentamer within the manufactured cell product (MP) and in peripheral blood from patient 202 at designated time points. **D,** Peripheral blood CD3$^+$ T cells flow sorted from PBMCs obtained from patient 202 at 28 months postinfusion (blue line) or from a healthy control transduced with NY-ESO-1^{c259}T cells (red line) demonstrate equivalent killing of A375 HLA-A2$^+$NY-ESO-1$^+$ target cells. Data plotted as mean of duplicate replicates ± SD.

differing levels of expression were observed, this observation may be attributed to tumor heterogeneity.

NY-ESO-1^{c259}T-cell Clonotype Mapping Using Next-Generation Sequencing of Endogenous *TCRBVs*

To probe the origin of the long-lived NY-ESO-1^{c259}T cells, *TCRBV* sequencing was performed on sorted, nontransduced CD8$^+$ subsets within the apheresis product and NY-ESO-1^{c259}CD8$^+$ subsets for patient 201, for whom ample cell numbers were available (Fig. 5A). Because the dextramer reagent used to identify NY-ESO-1^{c259}T cells binds more reliably to CD8$^+$ T cells compared with CD4$^+$ T cells, this analysis was limited to the CD8$^+$ subset. Where possible, naïve (N), TSCM, TCM, TEM, and TEMRA subsets were analyzed. NY-ESO-1^{c259}T cells bearing a TSCM phenotype (CCR7$^+$CD45RA$^+$) were nearly absent from the manufactured product but were found circulating postinfusion, whereas TEMRA cells, which constituted roughly 50% of the manufactured product, were present at low levels in the circulating pool postinfusion (Fig. 4C). Using the inverse Shannon entropy score as a measure of clonality, we observed that the TEM subset within the apheresis product and TEM cells in the manufactured product manifested diminished clonal diversity compared with other subsets, consistent with previous reports (26). Remarkably, however, postinfusion NY-ESO-1^{c259} N, TCM, TSCM, and TEMRA subsets demonstrated similar diversity to their nonengineered counterparts within the apheresis product and showed no evidence for clonal contraction over time. Similar results were observed for TCM and TEM populations in other patients (Supplementary Fig. S7). These findings are consistent with a model wherein the fitness of the NY-ESO-1^{c259}T-cell pool is similar to that of nontransduced T-cell subsets and wherein a robust regenerative pool maintains diversity of endogenous TCRs despite significant sustained expansion *in vivo*.

We next sought to track clonal progeny over time using the endogenous *TCRBV* sequence in NY-ESO-1^{c259}T cells as

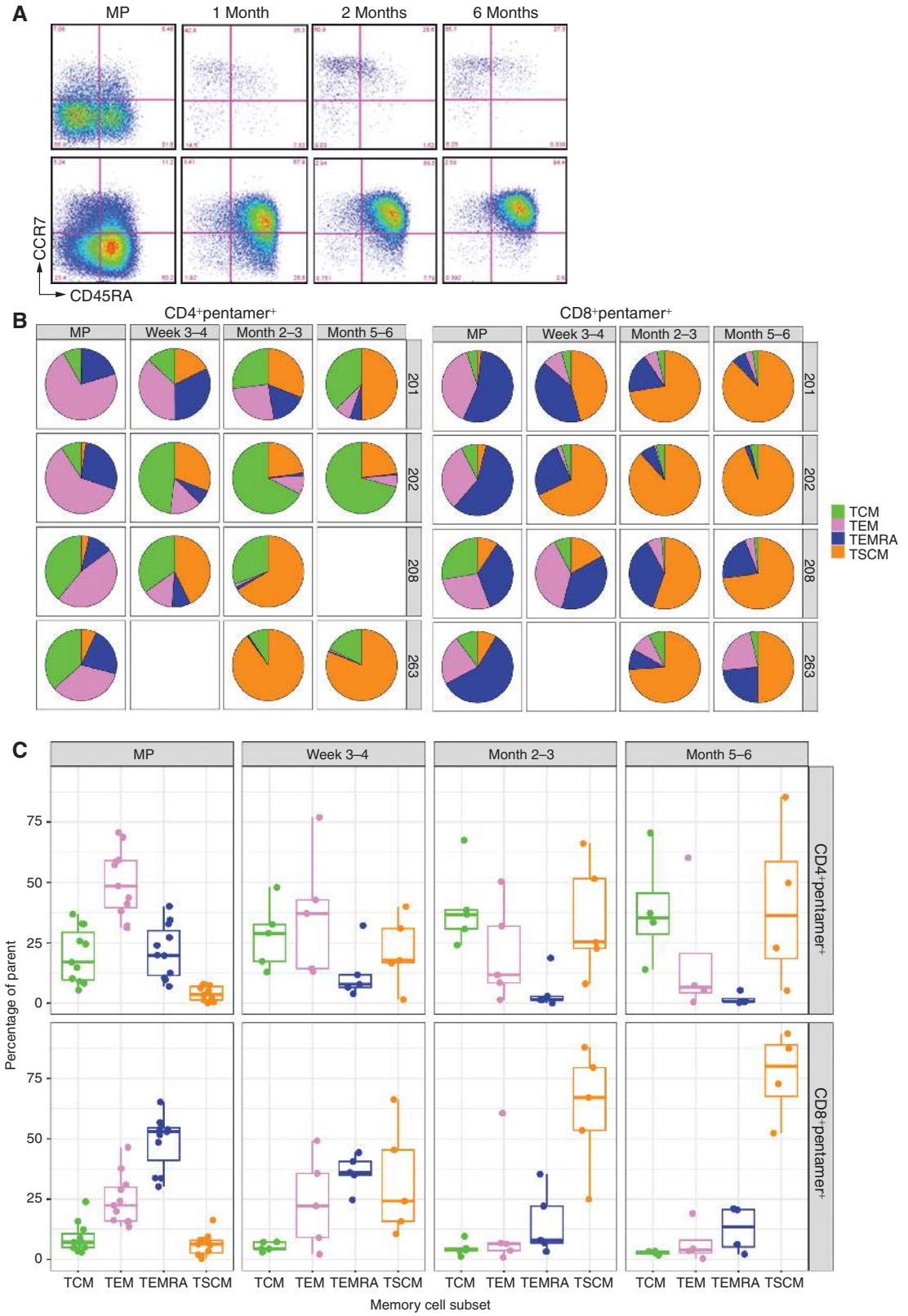

Figure 4. The NY-ESO-1^{c259}T-cell pool evolves from one composed predominantly of effector cells in the manufactured product to a long-term persisting pool composed predominantly of TCM and TSCM cells. **A,** Flow cytometry of pentamer binding CD4$^+$ (top) and CD8$^+$ (bottom) NY-ESO-1^{c259}T cells expressing CCR7 and CD45RA from patient 202 within the manufactured cell product (MP) and at the designated time points following infusion. **B** and **C,** Summarized data for 4 individual patients (**B**) and composite data from the entire cohort (**C**).

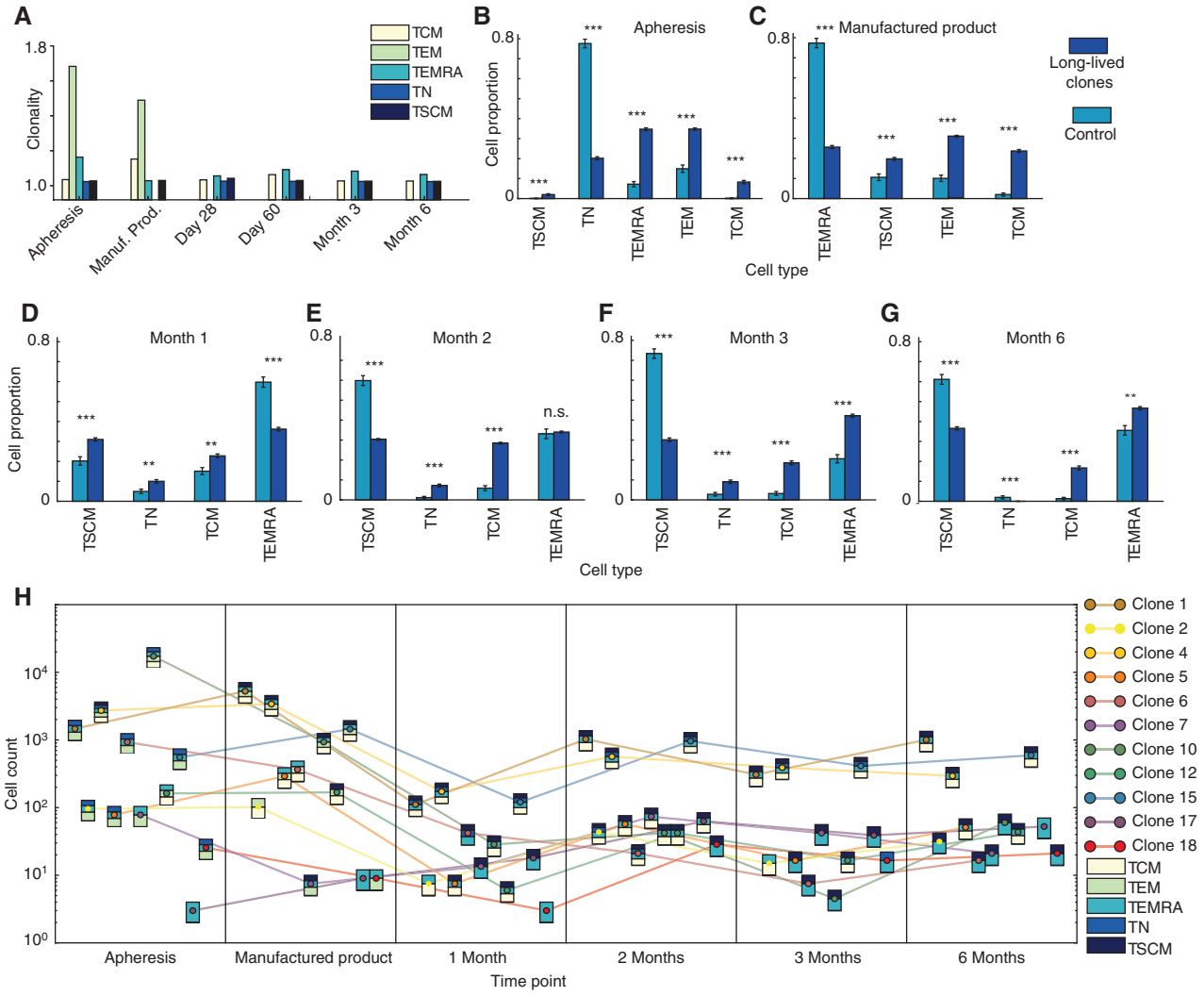

Figure 5. Longitudinal analysis of *TCRBV* sequences within sorted cell subsets. All cell samples are from patient 201. **A,** Clonality of each collected population at each time point. **B,** Average number of distinct long-lived clones (dark blue) and randomly selected control clones (light blue) present within each cell subset in the apheresis product. Over 1,000 bootstrapped samples from each group are selected then normalized to the total number of cells in each bootstrapped sample (19). **C–G,** The same as **B,** except clones represent NY-ESO-1^{c259}T cells in the manufactured product and at time points indicated in each graph. **H,** Cell counts of 11 long-lived clones elected based upon the presence of *TCRBV* sequences at each time point. Individual clones are connected across time, according to the legend at the top right. The cell subset containing an individual clone at a particular time point is denoted by the colored bars, according to the legend at the bottom right.

a barcode to identify cells with shared clonotypes and to compare subset distribution of long-lived versus random clonotypes. For these analyses, we used a cutoff of 10 copies of the unique *TCRBV* sequence present at the 6-month time point to define a "long-lived clonotype," and we used a bootstrap simulation to calculate the proportional subset distribution of 19 long-lived versus 19 randomly selected clonotypes (Fig. 5B and C). Results shown did not depend on the cutoff used. This approach controls for potential bias related to the increased proportion of specific subsets at particular time points (e.g., high levels of TEMRA in the manufactured product). The results revealed clear distinctions between the subset distribution of persistent versus random clonotypes at all time points (χ^2 test, $P < 0.01$). TCM subsets were enriched for persistent clonotypes at every time point examined (Fig. 5). TSCM subsets were enriched for persistent clonotypes in the apheresis product, manufactured product, and at 1-month postinfusion time points, but thereafter we observed a reduction. In addition, we also evaluated the distribution of persistent clones across cell subsets at each time point. We observed that the distribution of cell proportions was roughly uniform (and did not significantly diverge from a uniform distribution), whereas at 5 of 6 time points analyzed, the distribution of the random clones was significantly different from a uniform distribution.

Figure 5D illustrates the subset distribution and total number of 11 of the 19 persistent clones, selected because these clonotypes were identified at every time point analyzed. The data illustrate that persistent clonotypes are rarely found in only one

subset but rather are present in multiple T-cell subsets at each time point. Persistent clonotypes were predominantly found in both a regenerative subset (e.g., TSCM and/or TCM) as well as an effector subset at the same time point, including in the apheresis and manufactured product. This pattern would be expected if long-lasting clones were derived from a preexisting pool of antigen-experienced T cells with a presence in a self-maintaining regenerative pool that continually and efficiently gives rise to differentiated T-cell populations in response to antigen.

DISCUSSION

Adoptive cell therapy has emerged as one of the most promising approaches for harnessing the power of the immune response against cancer. Advances in vector design, receptor engineering, and cell production have improved the feasibility of generating activated T-cell products and diminished the time required to deliver products to patients. This progress is exemplified by the impressive results following CD19 chimeric antigen receptor (CAR) cell therapies for B-cell acute lymphoblastic leukemia and diffuse large B-cell lymphoma (27–32), the former of which uses a similar method of T-cell engineering and expansion as this study and has now been approved by the FDA. However, CAR-based therapeutics have not yet mediated benefit in significant numbers of patients with nonhematopoietic solid tumors. Adoptive transfer of tumor-infiltrating lymphocytes (TIL) can reproducibly mediate antitumor effects in melanoma, but TILs are difficult to generate from nonmelanoma histologies. Beyond small studies demonstrating activity of virus-specific TILs in cervical cancer (33) or a TIL product enriched for mutations in hepatobiliary carcinoma (34), the efficacy of adoptive therapy using TILs has not been convincingly demonstrated beyond melanoma. Engineered TCRs represent a promising approach to overcome the challenges associated with generating TILs and the theoretical limitations of low-affinity TCRs for tumor-associated self-antigens present in the natural T-cell repertoire (35).

In this study, safety, feasibility, and clinical and biological effects of autologous T cells engineered to express an affinity-enhanced TCR recognizing the NY-ESO-1–derived peptide SLLMWITQC (NY-ESO-1^{c259}T cells) were tested in synovial sarcoma. We demonstrate expansion of NY-ESO-1^{c259}T cells postinfusion in all patients and persistence of NY-ESO-1^{c259}T cells for 6 months in all responders and in 1 of 6 nonresponders. Previous studies of NY-ESO-1^{c259}T cells in synovial sarcoma reported similar response rates, but long-term persistence of NY-ESO-1^{c259}T cells was not reported. In addition, previously reported studies included administration of high-dose IL2, which is associated with significant toxicity (22, 23). In patients with relapsed or high-risk multiple myeloma, NY-ESO-1^{c259}T cells administered following a myeloablative preparative regimen in the context of an autologous stem cell transplant in an aging population demonstrated significant expansion and persistence associated with clinical benefit. Although clinical responses appeared greater than would be expected with transplant alone in the 20 patients studied, antitumor activity attributable to the infused cell product was difficult to definitively distinguish from the chemotherapy effect (36). A follow-on study is open to investigate the effect of the NY-ESO-1 SPEAR T cells without transplantation (NCT03168438). In the study presented here, NY-ESO-1^{c259}T cells administered without exogenous IL2 demonstrate impressive clinical activity associated with expansion and persistence following a reduced preparative regimen. Demonstration of transient increase in the size of metastatic lesions consistent with lymphocyte-induced inflammation followed by regression, trafficking of NY-ESO-1^{c259}T cells into the tumor bed, and a prolonged progressive clinical response in several patients confirms that the antitumor effects observed were immune-mediated. Responders demonstrated enhanced NY-ESO-1^{c259}T-cell expansion compared with nonresponders.

The impressive persistence of the NY-ESO-1^{c259}T cells in these patients, associated with continued antitumor effects *in vivo* and polyfunctionality *ex vivo*, provided an opportunity to more deeply analyze biological features associated with persistently functional T-cell populations following adoptive transfer. We observed dramatic differences between the subset composition of the NY-ESO-1^{c259}T-cell pool in the manufactured product, which nearly exclusively comprised TEM and TEMRA cells, versus the composition of the persisting NY-ESO-1^{c259}T-cell pool *in vivo*, which was comprised predominantly of TSCM and TCM subsets. Current models of CD8$^+$ T-cell differentiation hold that TEMRA and TEM cells derive from self-regenerating pools of naïve, TSCM, and/or TCM cells (37–40). According to these models, CD8$^+$ T-cell subset development is linear and hierarchical, such that naïve cells can generate naïve and/or TSCM cells, but TSCM cells do not generate naïve cells. Similarly, TSCM cells can generate TSCM and/or TCM cells, but TCM cells do not generate TSCM or naïve cells. Neither TEM cells nor TEMRA cells are capable of self-regeneration to any significant extent, thus explaining their inferiority for use in the setting of adoptive cell therapy (41, 42). We used fate mapping via next-generation sequencing of endogenous TCRs to test the veracity of this model as it relates to persisting NY-ESO-1^{c259}T cells following adoptive transfer.

Analysis of the diversity of endogenous TCRs in the NY-ESO-1^{c259}T cells expanding and persisting *in vivo* demonstrated similar repertoire diversity compared with nonengineered populations and no evidence of clonal contraction over time, demonstrating that a robust repertoire of T cells contributes to the NY-ESO-1^{c259}T-cell pool *in vivo*. This observation suggests that long-term persistence is independent of host factors that might drive survival through the endogenous TCR receptor, such as latent viruses like Epstein–Barr virus or cytomegalovirus. Such approaches have been exploited to assist in long-term engraftment of CAR T cells but are not likely to be at play here, because such a mechanism would be expected to increase the clonality of the persisting population, which was not observed (43, 44). The results also demonstrate that persistent T cells were not derived from one cell subset, but rather their clonotypes were present across all T-cell subsets examined, including naïve, TEM, TSCM, TCM, and TEMRA. These results, working within the traditional model of CD8$^+$ T-cell differentiation, lead to the conclusion that persisting clonotypes derive from a naïve subset, capable of both robust regeneration of naïve cells as well as efficient generation of progressively more differentiated subsets in response to

persistent antigen exposure *in vivo*. However, unexpectedly, persistent clonotypes were less enriched in the naïve subset of the preengineered apheresis product than random clonotypes. We were unable to perform this study in additional patients to establish this pattern more robustly, due to sample limitations. However, the data suggest it may be that current standard phenotypic profiles used to define T-cell subsets do not accurately identify pools with capabilities limited to the hierarchical, linear differentiation model described above.

A common feature of clinical studies that demonstrate prolonged persistence of engineered T cells is use of a manufacturing method that simultaneously provides activation and costimulation to the manufactured T cells (45–47). Costimulation through the CD28 molecule increases metabolic capacity of T cells, their telomerase activity, and the antiapoptotic protein BCL-X(L), which contribute to activity and longevity of the infused cells (48–50). Fate mapping, such as that performed here, cannot precisely determine the subset from which individual effectors are derived. Nonetheless, the observation that persistent clonotypes were consistently enriched within naïve, TSCM, and TCM pools compared with random clonotypes provides evidence that phenotypes identified previously to define these pools identify subsets with enhanced regenerative capacity. This raises the prospect that administering selected populations of regenerative populations in future trials may enable dose reduction and potentially enhanced efficacy. Furthermore, the observation that persistent clonotypes distribute more uniformly across regenerative and effector subsets than random clonotypes, due to the efficient generation of effector pools, illustrates that NY-ESO^{c259}T exhibits a balance of efficient effector T-cell generation and robust self-renewal.

The results reported herein provide evidence that adoptive T-cell therapy for cancer using an affinity-enhanced TCR, without IL2, can provide a robust and long-lasting pool of antitumor effectors that can mediate clinically meaningful antitumor effects. The NY-ESO-1^{c259}T cells maintained killing potential and demonstrated no evidence for T-cell exhaustion in the peripheral blood compartment, despite prolonged persistence and exposure to antigen *in vivo*. Further analyses revealed evolution from an infused pool comprised predominantly of effector cells to a persisting pool dominated by TCM and TSCM subsets. Next-generation *TRBV* sequencing of sorted cell subsets confirmed enrichment of persistent NY-ESO-1^{c259}T-cell clonotypes in TCM subsets at all time points analyzed and enrichment within TSCM subsets. The data presented are consistent with a model wherein the engineered NY-ESO-1^{c259}T-cell products administered in this trial contained a stem/progenitor pool capable of both self-renewal and prolonged efficient generation of potent antitumor effectors.

METHODS

Study Design

The data and results presented are from Cohort 1 of an ongoing pilot, phase I/II, nonrandomized, open-label study (NCT01343043). This study was conducted in compliance with the Declaration of Helsinki (with amendments), and in accordance with local legal and regulatory requirements. Patients were recruited from 3 academic centers in the United States. The protocol was approved by each center's Institutional Review Board, and all patients signed informed consent forms. Enrollment for the cohort reported has been completed. Of the other 3 cohorts in the study, 2 are ongoing and 1 has been terminated. The results from these 3 cohorts will be reported following study completion.

The primary endpoint was ORR, which was defined as the proportion of patients with a confirmed CR or PR. Secondary endpoints assessing efficacy include the following: time to response (time from T-cell infusion to earliest documentation of confirmed PR or CR), duration of response (time from first documented evidence of confirmed CR or PR to the earliest documentation of disease progression or death from any cause), PFS (time from T-cell infusion to the earliest documentation of disease progression or death from any cause), and the OS rate (time from T-cell infusion to death from any cause). Additional endpoints were safety and tolerability of NY-ESO-1^{c259}T as well as correlative studies to evaluate expansion and persistence of gene-marked cells and the T-cell subsets.

Patients

Key eligibility criteria included patients 4 years or older who have histologically confirmed synovial sarcoma that is unresectable, metastatic, progressive, persistent, or recurrent (advanced disease), are HLA*02 positive, and have tumors that express NY-ESO-1 tumor antigen (≥50% of tumor cells express 2+ or 3+ staining by IHC). Although various HLA*02 haplotypes bind the target peptide and are then recognized by the NY-ESO-1^{c259}TCR, the affinity of this binding varies. Patients in this cohort were HLA*02:01 or HLA-A2*02:06, which have similar binding affinities. Patients must have previously received an ifosfamide and/or doxorubicin-containing regimen and have measurable disease according to RECIST version 1.1. Patients had Eastern Cooperative Oncology Group performance status 0 to 1 or for children ≤10 years of age Lansky ≥60, had a life expectancy of >3 months, and had left ventricular ejection fraction of ≥40%. Laboratory assessments for eligibility were as follows: absolute neutrophil count ≥1,000/mm^3, platelet count ≥75,000/mm^3, serum bilirubin <2 mg/dL, ALT and AST ≤2.5× upper limit of normal, and creatinine clearance of ≥60 mL/minute. HLA by high-resolution testing was performed at a local or central laboratory. NY-ESO-1 testing was performed at a Clinical Laboratory Improvement Amendments (CLIA)–certified pathology laboratory at the NCI, Bethesda, MD. Disease was classified according to RECIST v 1.1, and radiological disease assessments were performed at weeks 4, 8, 12, and every 3 months thereafter. Patients who progressed were followed up for long-term toxicity until death or for 15 years postinfusion.

Cell and Vector Manufacturing

Cells and vector were manufactured as described previously (36).

Cell Manufacturing. Engineered T cells were manufactured at the Cell and Vaccine Production Facility at the University of Pennsylvania (Philadelphia, PA) for patients 201 and 202. The remaining patients' cells were manufactured at Progenitor Cell Therapy, following qualification of the transferred process. Engineered T cells were generated from CD25-depleted CD4$^+$ and CD8$^+$ T cells that were activated and expanded using αCD3/αCD28 antibody-conjugated beads (Life Technologies). T cells were transduced at a multiplicity of infection of 1 transducing unit per cell. Manufacturing time ranged from 28 to 35 days, including release testing.

Vector Manufacturing. The lentiviral vector is a self-inactivating vector derived from HIV-1 containing a woodchuck hepatitis virus posttranscriptional regulatory element (WPRE). An EF1α promoter drives transgene expression. Vector was produced at the City of Hope (Duarte, CA) using transient transfection with four plasmids expressing the transfer vector, rev, VSV-G, and gag/pol, in 293T cells. Supernatant

was collected at multiple time points, clarified, treated with Benzonase, and concentrated by tangential flow filtration and centrifugation. Transduction potency was measured on primary T cells.

Cell Lines and Normal Primary Human Cells

The NY-ESO-1–expressing A375 tumor cell line was obtained from the ATCC (February 2016). Cells have been routinely screened for *Mycoplasma* contamination (Mycoplasma Experience Ltd.) and authenticated by short tandem repeat (STR) analysis (LGC Standards). The cells were last authenticated by STR analysis in January 2017. Peripheral blood lymphocytes were obtained from human healthy volunteers following Ficoll–Hypaque density gradient separation (Lymphoprep, Nycomed Pharma AS). T cells from healthy donors were activated, expanded, and transduced identically to the clinical manufacturing process.

Assays for Gene-Modified T-cell Persistence and Phenotypic Analysis

Research sample collection and initial processing were performed at clinical sites and then transferred to Cambridge Biomedical, a commercial laboratory operating in compliance with Good Laboratory Practices (GLP), as described previously (36), for further processing and qPCR analyses. For multiparametric flow cytometric analyses, samples were subsequently sent to Caprion, a commercial GLP-compliant laboratory. Assay performance and data reporting conforms with MIATA guidelines (51).

Sample Draws and Processing. Samples were collected as described previously (36). Peripheral blood samples were collected in sodium heparin CPT tubes (BD Vacutainer) for qPCR analysis or flow cytometric analysis. Samples were delivered to the commercial laboratory from the clinical sites at room temperature and in insulated containers. For flow cytometric analyses, PBMCs were purified, processed, and stored in liquid nitrogen prior to transfer to the commercial laboratory.

qPCR Analyses. Genomic DNA was isolated from PBMCs via QIAamp DNA Blood Mini Kit (Qiagen), quantified by spectrophotometer, and stored until testing at −80°C. qPCR analyses were performed in bulk and in triplicate for each time point using ABI TaqMan technology (6FAM-labeled WPRE probe with MGB quencher) and a validated assay to detect the WPRE sequence present in the lentivirus backbone, using 100 ng genomic DNA per replicate. A standard curve was established using serial dilutions of a plasmid containing the WPRE sequence. The limit of detection for the assay is 100 copies/μg genomic DNA. The white blood cell count was used as an amplifier to calculate the number of gene modified cells in the blood. An assumption of 1 vector copy per transduced cell was based upon the multiplicity of infection of 1 used for cell transduction; however, the gene modified cell population is likely to contain a subset of cells with multiple integration events.

Multiparametric Flow Cytometry. Following receipt at a commercial laboratory, cells were stored in liquid nitrogen vapor phase and thawed on the day of assay. Multiparametric immunophenotyping was performed using approximately 1×10^6 cells/condition. Cells were acquired using a BD LSR II cytometer (BD Biosciences). Compensation values were established using single antibody stains and BD compensation beads (BD Biosciences). Data were analyzed using FlowJo v9.6.2 (Treestar), R v3.3.1 (R Foundation for Statistical Computing; ref. 52), Pestle (NIH), and SPICE (NIH) software packages.

Flow Cytometry Detection Reagents. The following antibodies were used for T-cell phenotyping: CD8-BV650 (BD), CD4-BV605 (BD Biosciences), CD3-Alexa Fluor700 (BD Biosciences), CD95-BV711 (BD Biosciences), CD45RO-PerCPCy5.5 (BD Biosciences), CD25-APC-Cy7 (BD Biosciences), CD127-BV421 (BioLegend), CCR7-PE-Cy7 (BioLegend), CD45RA-ECD (Beckman Coulter), PD-1-BV785 (BioLegend), LAG3-FITC (R&D Systems), and TIM3-APC (R&D Systems). The dead cell exclusion stain (Live/Dead Aqua) was purchased from Invitrogen. To detect transduced NY-ESO-1^{c259}TCR-expressing cells, PE-conjugated pentamer reagents specific for the HLA-A*02:01 SLLMWITQC complex (ProImmune) were used at the manufacturer's recommended concentrations.

FACS

Frozen patient PBMCs and healthy donor NY-ESO-1 TCR transduced T cells were thawed in RPMI with 10% FBS. These cells were then stained with a pentamer specific to NY-ESO-1^{c259}TCR-transduced T cells (A*02:01 SLLMWITQC) for 20 minutes at 4°C, followed by subsequent staining with antibodies for an additional 15 minutes at 4°C. 7-AAD was used as the live/dead marker and was added at least 10 minutes prior to sorting. Fluorescence minus one controls were prepared and used for correct gate compensation settings. Cells were sorted using an Aria Fusion cell sorter (BD Biosciences). Data were analyzed using FACSDiva (BD Biosciences) software postsort. The following antibodies were used for identification of transduced T cells for sorting and subsequent postsort phenotypic analysis: CD8-QDOT655 (Life Technologies), CD4-AF780 (eBioscience), CD3-AF700 (eBioscience), CCR7-PE-CF594 (BD Biosciences) and CD45RA-FITC (eBioscience), CD127-BV421 (BioLegend), CD95-BV711 (BD Biosciences). The NY-ESO-1 Pro5 MHC-pentamer conjugated to PE (A*02:01 SLLMWITQC) was purchased from ProImmune. For lineage-tracing studies, NY-ESO-1 TCR-transduced T cells were stained with NY-ESO-1 dextramer conjugated to PE (A*02:01 SLLMWITQC) and purchased from Immudex. 7-AAD was purchased from BD Biosciences.

Cytotoxicity

Killing assays were carried out with the IncuCyte FLR-Platform (Essen BioScience), as described previously (53, 54). Adherent A375 cells were plated at 2×10^4 cells per well and incubated overnight at 37°C/5% CO_2 in RPMI-1640 medium supplemented with 10% heat-inactivated FBS and GlutaMAX (Life Technologies) in a 96-well flat-bottom plate. The following day, cells were washed twice and incubated with 3×10^4 sorted NY-ESO-1^{c259}TCR-transduced T cells from either a patient or healthy donor per well and 3.3 μmol/L IncuCyte Caspase-3/7 reagent (Essen BioScience). Cells were imaged over 130 hours at 3-hour intervals to detect apoptosis. Data were analyzed using IncuCyte ZOOM 2015A software (Essen BioScience) to distinguish apoptotic A375 cells from apoptotic T cells.

IHC

Serial 5-μm sections of formalin-fixed, paraffin-embedded tissues were analyzed for the following single markers by IHC: NY-ESO-1, Pan-CK (Clone AE1/AE3/PCK26, Ventana), CD45 (Clone 2B11 + PD7/26, Ventana), CD3 (Clone 2GV6, Ventana), CD8 (Clone C8/144B, Dako), CD4 (Clone 1F6, Novocastra), PD-L1 (Clone SP142, Ventana), and PD-1 (Clone SP269, Spring Bioscience). Staining was performed either at a CLIA-certified clinical laboratory (QualTek Labs) or a CLIA-certified and Belgian Accreditation Organization and College of American Pathologists–accredited laboratory (HistoGeneX). For some samples, NY-ESO-1 IHC testing was performed at the NCI (Bethesda, MD).

Immunofluorescence Staining

Double immunofluorescence (IF) labeling assays were performed at a commercial laboratory on the Ventana Discovery XT platform. In the first assay, 5 μm–thick sections were incubated for 2 hours at 37°C with a mix of mouse monoclonal anti-human CD8 (Clone C8/144B,

1/100, DakoCytomation) and rabbit monoclonal anti-human Ki67 (Clone 30.9, 1/4, Ventana). Visualization was performed using Alexa488-labeled goat anti-mouse (1/100, Molecular Probes) and Cy3-labeled goat anti-rabbit (1/1,000, Jackson Immunoresearch Laboratories) antibodies. The second immunofluorescent assay combined rabbit monoclonal anti-human CD3 (clone 2GV6, 1/4, Ventana) with mouse monoclonal FoxP3 (clone 236A/E7, 1/60, eBioscience). Visualization was established using Cy3-labeled goat anti-mouse (1/100, Jackson Immunoresearch Laboratories) and Alexa488-labeled goat anti-rabbit (1/100, Invitrogen Molecular Probes) antibodies. Counterstain for both assays was performed using Hoechst 33342 (1/2,000, Invitrogen Molecular Probes). As a negative control, host immunoglobulins (negative control mouse, clone M1G-45, 1/60–1/200, Abcam and negative control rabbit, 1/5,000–1/25,000, Cell Signaling Technologies) were used to replace the primary antibody.

IF Imaging

Virtual images were generated using ZEN 2 blue edition software (Carl Zeiss Microscopy GmbH 2011) on an Axio Scan.Z1 Imaging microscope (Carl Zeiss) using the same exposure times for all samples. Each image consisted of 3 image layers, one for each fluorescent tag (layer 1 for FOXP3/Ki67, layer 2 for CD3/CD8, layer 3 for Hoechst). IF images were quantified within a pathologist-defined tumor region via object-oriented image analysis using Definiens Architect XD v2.1.1 Tissue Studio IF with action library v3.6.1 (Definiens). A specific rule set was written in Definiens Architect XD v2.1.1 Tissue Studio IF to determine the total number of nuclei with expression of signal in layer 1 (FOXP3 or Ki67) and/or layer 2 (CD3 or CD8) of the image. Manual delineation of the tumor region, guided by a histopathology report, was done in Definiens Architect XD v2.1.1 Tissue Studio IF. Artifacts due to tissue processing and whole-slide imaging, such as autofluorescence, tissue tearing, tissue folding, and out-of-focus regions, were excluded. Nuclear objects were generated by Definiens Architect XD v2.1.1 Tissue Studio IF based on the Hoechst layer (layer 3) of the image and the expression of signal present on the other two image layers (layer 1 and layer 2) was evaluated within these nuclear objects. The analysis method considered signals to be positive when signals above the background level (determined via an IgG isotype control) were present.

Brightfield Imaging

All stained slides were scanned with whole-slide scanner 250 Flash II (3DHISTECH) to obtain a whole-slide image. A 20 × Plan Apo objective (0.80 numerical aperture) and a CIS (VCC-FC60FR19CL) charge-coupled device progressive scan color camera with a resulting image resolution of 0.24 μm/pixel was used. JPEG image encoding with quality factor 80 and an interpolated focus distance of 15 with stitching in the scan options were chosen. For every slide, a specific scan profile was configured. Scanned images were examined in Pannoramic Viewer (3DHISTECH) to check for image quality and whole-tissue coverage.

Object-based image analysis for Pan-CK, CD45, CD3, CD8, CD4, CD163, CD20, PD-L1, and PD-1 was done with the commercial software VIS version 6.2 (Visiopharm) at a commercial laboratory. Manual delineation of the tumor region, guided by a histopathology report, was done in the Image Analysis module of VIS. Artifacts due to tissue processing and whole-slide imaging, such as ruptured tissue, dirt, or out-of-focus regions, were excluded. For every marker, an APP was written that calculated the area of the manually delineated tumor region and the area of the marker-positive regions.

TCR Vβ Sequencing

Flow-sorted populations of cells were snap-frozen on dry ice and submitted for either Survey or Deep resolution sequencing of the CDR3 regions of TCRβ and/or TCRα (immunoSEQ, Adaptive Biotechnologies). Briefly, genomic DNA was extracted from these dry pellets and subjected to multiplexed amplification of TCR sequences using proprietary combinations of V and J gene primers, which are validated to reduce amplification bias. The resulting amplification products were used for next-generation sequencing through the CDR3 region, such that read counts for a given clonally rearranged TCR sequence allow quantification of clone size.

Longitudinal Analysis of TCR Sequences from Sorted Cell Populations

Clonality is calculated as the inverse normalized Shannon entropy, defined as $\frac{1}{-\frac{1}{\log_2 N}\sum_i p_i \log_2 p_i}$, where N is the total number of unique clones and p_i is the proportion of clone i. A clone is defined as long-lived if there are more than 10 copies of that clone at the month 6 time point. Results described are not sensitive to the particular threshold defining a long-lived clone. For the sample considered herein, there were 19 long-lived clones.

At each time point, a bootstrapped collection of 19 long-lived clones or control clones (uniformly selected from all clones present) was simulated from the entire set of clones present at that time across all cell types. The proportion of this sample with at least one copy found in each cell subtype was calculated. Clones found in multiple cell subsets were counted toward each. One thousand bootstrapped samples were performed at each time point for both long-lived and control samples, and the results of this calculation were not sensitive to this parameter. Significance was determined with a two-tailed Student t test, and P values were corrected for multiple hypothesis testing via the Bonferroni method.

Statistical Analyses

The primary endpoint is ORR per RECIST v1.1, defined as the proportion of subjects with a confirmed CR or PR relative to the total number of subjects. The ORR was based on confirmed responses from the investigator assessment of overall response. Subjects with unknown or missing response were treated as nonresponders; that is, they were included in the denominator when calculating the proportion. The ORR was evaluated using 95% Clopper–Pearson confidence intervals. The primary analysis population was the modified intention-to-treat population, defined as subjects who received the NY-ESO-1^{c259}T-cell therapy.

The secondary endpoints of peak expansion, time to response, duration of overall response, PFS, and OS were evaluated using descriptive statistics and/or graphical displays such as line plots, box plots, or Kaplan–Meier curves, as appropriate. Peak expansion is the maximum persistence value after NY-ESO-1^{c259}T-cell infusion for each subject. Time to response is defined as the interval between NY-ESO-1^{c259}T-cell infusion and earliest date of first documented confirmed response. Duration of overall response is defined as the time from confirmed response until the first date of progressive disease per RECIST v1.1. OS is defined as the interval between the date of NY-ESO-1^{c259}T-cell infusion and death due to any cause. For this data cutoff, if the subject was known to be alive on March 30, 2017, OS was censored at this date. Median survival was calculated using the log–log estimate and the corresponding 95% confidence interval. Peak expansion was compared between subjects who responded and did not respond to NY-ESO-1^{c259}T-cell therapy using the exact based Wilcoxon test. Flow cytometry was assessed using the Friedman test.

Disclosure of Potential Conflicts of Interest

Sandra P. D'Angelo reports receiving commercial research support from Adaptimmune. J. Glod is a consultant/advisory board member for GSK. S.A. Grupp reports receiving commercial research support from Adaptimmune and is a consultant/advisory board member for the same. W.D. Tap is a consultant/advisory board member for Adaptimmune

and Immune Design. S. Basu has ownership interest (including patents) in Adaptimmune LLC. G. Kari has ownership interest (including patents) in Adaptimmune. T. Holdich has ownership interest in Adaptimmune (share options). C.L. Mackall is a member of the Adaptimmune Scientific Advisory Board. No potential conflicts of interest were disclosed by the other authors.

Authors' Contributions

Conception and design: S.P. D'Angelo, L. Melchiori, M.S. Merchant, S. Grupp, K. Chagin, G.K. Binder, H. Zhang, T. Trivedi, L. Pandite, C.L. Mackall

Development of methodology: L. Melchiori, M.S. Merchant, R. Kaplan, S. Basu, N. Bath, G. Betts, H. Zhang, T. Trivedi

Acquisition of data (provided animals, acquired and managed patients, provided facilities, etc.): S.P. D'Angelo, L. Melchiori, M.S. Merchant, J. Glod, R. Kaplan, S. Grupp, W.D. Tap, N. Bath, A. Tipping, G. Betts, I. Ramachandran, H. Zhang, E. Van Winkle, T. Holdich, R. Amado, C.L. Mackall

Analysis and interpretation of data (e.g., statistical analysis, biostatistics, computational analysis): S.P. D'Angelo, L. Melchiori, M.S. Merchant, W.D. Tap, K. Chagin, G.K. Binder, S. Basu, D.E. Lowther, R. Wang, A. Tipping, J.-M. Navenot, H. Zhang, D.K. Wells, T. Trivedi, T. Holdich, L. Pandite, R. Amado, C.L. Mackall

Writing, review, and/or revision of the manuscript: S.P. D'Angelo, L. Melchiori, M.S. Merchant, J. Glod, R. Kaplan, S. Grupp, W.D. Tap, K. Chagin, G.K. Binder, S. Basu, D.E. Lowther, I. Ramachandran, J.-M. Navenot, H. Zhang, D.K. Wells, E. Van Winkle, G. Kari, T. Trivedi, T. Holdich, L. Pandite, R. Amado, C.L. Mackall

Administrative, technical, or material support (i.e., reporting or organizing data, constructing databases): L. Melchiori, D. Bernstein, K. Chagin, S. Basu, H. Zhang, E. Van Winkle

Study supervision: M.S. Merchant, S. Grupp, W.D. Tap, K. Chagin, G.K. Binder, L. Pandite, C.L. Mackall

Other (clinical operations for the study): G.K. Binder

Acknowledgments

We are grateful to the patients who participated in this study. This trial is registered on ClinicalTrials.gov, identifier NCT01343043. This work was supported, in part, by the Intramural Research Program of the NCI. This clinical trial was sponsored by Adaptimmune.

Received December 18, 2017; revised April 24, 2018; accepted May 18, 2018; published first June 11, 2018.

REFERENCES

1. Brennan MF, Antonescu CR, Maki RG. Management of soft tissue sarcoma. New York, NY: Springer; 2012.
2. Hodi FS, O'Day SJ, McDermott DF, Weber RW, Sosman JA, Haanen JB, et al. Improved survival with ipilimumab in patients with metastatic melanoma. N Engl J Med 2010;363:711–23.
3. Ansell SM, Lesokhin AM, Borrello I, Halwani A, Scott EC, Gutierrez M, et al. PD-1 blockade with nivolumab in relapsed or refractory Hodgkin's lymphoma. N Engl J Med 2015;372:311–9.
4. Brahmer J, Reckamp KL, Baas P, Crino L, Eberhardt WE, Poddubskaya E, et al. Nivolumab versus docetaxel in advanced squamous-cell non-small-cell lung cancer. N Engl J Med 2015;373:123–35.
5. Powles T, Eder JP, Fine GD, Braiteh FS, Loriot Y, Cruz C, et al. MPDL3280A (anti-PD-L1) treatment leads to clinical activity in metastatic bladder cancer. Nature 2014;515:558–62.
6. Topalian SL, Drake CG, Pardoll DM. Immune checkpoint blockade: a common denominator approach to cancer therapy. Cancer Cell 2015;27:450–61.
7. Topalian SL, Hodi FS, Brahmer JR, Gettinger SN, Smith DC, McDermott DF, et al. Safety, activity, and immune correlates of anti-PD-1 antibody in cancer. N Engl J Med 2012;366:2443–54.
8. Schumacher TN, Schreiber RD. Neoantigens in cancer immunotherapy. Science 2015;348:69–74.
9. McGranahan N, Furness AJ, Rosenthal R, Ramskov S, Lyngaa R, Saini SK, et al. Clonal neoantigens elicit T cell immunoreactivity and sensitivity to immune checkpoint blockade. Science 2016;351:1463–9.
10. Rizvi NA, Hellmann MD, Snyder A, Kvistborg P, Makarov V, Havel JJ, et al. Cancer immunology. mutational landscape determines sensitivity to PD-1 blockade in non-small cell lung cancer. Science 2015;348:124–8.
11. Le DT, Uram JN, Wang H, Bartlett BR, Kemberling H, Eyring AD, et al. PD-1 blockade in tumors with mismatch-repair deficiency. N Engl J Med 2015;372:2509–20.
12. Alexandrov LB, Nik-Zainal S, Wedge DC, Aparicio SA, Behjati S, Biankin AV, et al. Signatures of mutational processes in human cancer. Nature 2013;500:415–21.
13. Burgess M, Crowley J, Reinke D, Riedel R, George S, Movva S, et al. SARC 028: a phase II study of the anti-PD1 antibody pembrolizumab (P) in patients (Pts) with advanced sarcomas. J Clin Oncol 2015;33:15s, (suppl; abstr TPS10578).
14. Jungbluth AA, Chen YT, Stockert E, Busam KJ, Kolb D, Iversen K, et al. Immunohistochemical analysis of NY-ESO-1 antigen expression in normal and malignant human tissues. Int J Cancer 2001;92:856–60.
15. Satie AP, Rajpert-De Meyts E, Spagnoli GC, Henno S, Olivo L, Jacobsen GK, et al. The cancer-testis gene, NY-ESO-1, is expressed in normal fetal and adult testes and in spermatocytic seminomas and testicular carcinoma in situ. Lab Invest 2002;82:775–80.
16. Lai JP, Robbins PF, Raffeld M, Aung PP, Tsokos M, Rosenberg SA, et al. NY-ESO-1 expression in synovial sarcoma and other mesenchymal tumors: significance for NY-ESO-1-based targeted therapy and differential diagnosis. Mod Pathol 2012;25:854–8.
17. Kawada J, Wada H, Isobe M, Gnjatic S, Nishikawa H, Jungbluth AA, et al. Heteroclitic serological response in esophageal and prostate cancer patients after NY-ESO-1 protein vaccination. Int J Cancer 2012;130:584–92.
18. Eikawa S, Kakimi K, Isobe M, Kuzushima K, Luescher I, Ohue Y, et al. Induction of CD8 T-cell responses restricted to multiple HLA class I alleles in a cancer patient by immunization with a 20-mer NY-ESO-1f (NY-ESO-1 91-110) peptide. Int J Cancer 2013;132:345–54.
19. Takeoka T, Nagase H, Kurose K, Ohue Y, Yamasaki M, Takiguchi S, et al. NY-ESO-1 protein cancer vaccine with poly-ICLC and OK-432: rapid and strong induction of NY-ESO-1-specific immune responses by poly-ICLC. J Immunother 2017 Mar 23. [Epub ahead of print].
20. Kakimi K, Isobe M, Uenaka A, Wada H, Sato E, Doki Y, et al. A phase I study of vaccination with NY-ESO-1f peptide mixed with Picibanil OK-432 and Montanide ISA-51 in patients with cancers expressing the NY-ESO-1 antigen. Int J Cancer 2011;129:2836–46.
21. Wada H, Isobe M, Kakimi K, Mizote Y, Eikawa S, Sato E, et al. Vaccination with NY-ESO-1 overlapping peptides mixed with Picibanil OK-432 and montanide ISA-51 in patients with cancers expressing the NY-ESO-1 antigen. J Immunother 2014;37:84–92.
22. Robbins PF, Kassim SH, Tran TL, Crystal JS, Morgan RA, Feldman SA, et al. A pilot trial using lymphocytes genetically engineered with an NY-ESO-1-reactive T-cell receptor: long-term follow-up and correlates with response. Clin Cancer Res 2015;21:1019–27.
23. Robbins PF, Morgan RA, Feldman SA, Yang JC, Sherry RM, Dudley ME, et al. Tumor regression in patients with metastatic synovial cell sarcoma and melanoma using genetically engineered lymphocytes reactive with NY-ESO-1. J Clin Oncol 2011;29:917–24.
24. Pollack SM, Jungbluth AA, Hoch BL, Farrar EA, Bleakley M, Schneider DJ, et al. NY-ESO-1 is a ubiquitous immunotherapeutic target antigen for patients with myxoid/round cell liposarcoma. Cancer 2012;118:4564–70.
25. Zhao Y, Bennett AD, Zheng Z, Wang QJ, Robbins PF, Yu LY, et al. High-affinity TCRs generated by phage display provide CD4+ T cells with the ability to recognize and kill tumor cell lines. J Immunol 2007;179:5845–54.
26. Suessmuth Y, Mukherjee R, Watkins B, Koura DT, Finstermeier K, Desmarais C, et al. CMV reactivation drives posttransplant T-cell reconstitution and results in defects in the underlying TCRbeta repertoire. Blood 2015;125:3835–50.

27. Davila ML, Riviere I, Wang X, Bartido S, Park J, Curran K, et al. Efficacy and toxicity management of 19-28z CAR T cell therapy in B cell acute lymphoblastic leukemia. Sci Transl Med 2014;6:224ra25.
28. Maude SL, Frey N, Shaw PA, Aplenc R, Barrett DM, Bunin NJ, et al. Chimeric antigen receptor T cells for sustained remissions in leukemia. N Engl J Med 2014;371:1507–17.
29. Lee DW, Kochenderfer JN, Stetler-Stevenson M, Cui YK, Delbrook C, Feldman SA, et al. T cells expressing CD19 chimeric antigen receptors for acute lymphoblastic leukaemia in children and young adults: a phase 1 dose-escalation trial. Lancet 2015;385:517–28.
30. Kochenderfer JN, Dudley ME, Kassim SH, Somerville RP, Carpenter RO, Stetler-Stevenson M, et al. Chemotherapy-refractory diffuse large B-cell lymphoma and indolent B-cell malignancies can be effectively treated with autologous T cells expressing an anti-CD19 chimeric antigen receptor. J Clin Oncol 2015;33:540–9.
31. Turtle CJ, Hanafi LA, Berger C, Gooley TA, Cherian S, Hudecek M, et al. CD19 CAR-T cells of defined CD4+:CD8+ composition in adult B cell ALL patients. J Clin Invest 2016;126:2123–38.
32. Turtle CJ, Hanafi LA, Berger C, Hudecek M, Pender B, Robinson E, et al. Immunotherapy of non-Hodgkin's lymphoma with a defined ratio of CD8+ and CD4+ CD19-specific chimeric antigen receptor-modified T cells. Sci Transl Med 2016;8:355ra116.
33. Stevanovic S, Draper LM, Langhan MM, Campbell TE, Kwong ML, Wunderlich JR, et al. Complete regression of metastatic cervical cancer after treatment with human papillomavirus-targeted tumor-infiltrating T cells. J Clin Oncol 2015;33:1543–50.
34. Tran E, Turcotte S, Gros A, Robbins PF, Lu YC, Dudley ME, et al. Cancer immunotherapy based on mutation-specific CD4+ T cells in a patient with epithelial cancer. Science 2014;344:641–5.
35. Aleksic M, Liddy N, Molloy PE, Pumphrey N, Vuidepot A, Chang KM, et al. Different affinity windows for virus and cancer-specific T-cell receptors: implications for therapeutic strategies. Eur J Immunol 2012;42:3174–9.
36. Rapoport AP, Stadtmauer EA, Binder-Scholl GK, Goloubeva O, Vogl DT, Lacey SF, et al. NY-ESO-1-specific TCR-engineered T cells mediate sustained antigen-specific antitumor effects in myeloma. Nat Med 2015;21:914–21.
37. Gattinoni L, Lugli E, Ji Y, Pos Z, Paulos CM, Quigley MF, et al. A human memory T cell subset with stem cell-like properties. Nat Med 2011;17:1290–7.
38. Gattinoni L, Klebanoff CA, Restifo NP. Paths to stemness: building the ultimate antitumour T cell. Nat Rev Cancer 2012;12:671–84.
39. Gerlach C, van Heijst JW, Swart E, Sie D, Armstrong N, Kerkhoven RM, et al. One naive T cell, multiple fates in CD8+ T cell differentiation. J Exp Med 2010;207:1235–46.
40. Gerlach C, van Heijst JW, Schumacher TN. The descent of memory T cells. Ann N Y Acad Sci 2011;1217:139–53.
41. Klebanoff CA, Gattinoni L, Torabi-Parizi P, Kerstann K, Cardones AR, Finkelstein SE, et al. Central memory self/tumor-reactive CD8+ T cells confer superior antitumor immunity compared with effector memory T cells. Proc Natl Acad Sci U S A 2005;102:9571–6.
42. Gattinoni L, Klebanoff CA, Palmer DC, Wrzesinski C, Kerstann K, Yu Z, et al. Acquisition of full effector function *in vitro* paradoxically impairs the *in vivo* antitumor efficacy of adoptively transferred CD8+ T cells. J Clin Invest 2005;115:1616–26.
43. Cruz CR, Micklethwaite KP, Savoldo B, Ramos CA, Lam S, Ku S, et al. Infusion of donor-derived CD19-redirected virus-specific T cells for B-cell malignancies relapsed after allogeneic stem cell transplant: a phase 1 study. Blood 2013;122:2965–73.
44. Rossig C, Pule M, Altvater B, Saiagh S, Wright G, Ghorashian S, et al. Vaccination to improve the persistence of CD19CAR gene-modified T cells in relapsed pediatric acute lymphoblastic leukemia. Leukemia 2017;31:1087–95.
45. Barrett DM, Singh N, Liu X, Jiang S, June CH, Grupp SA, et al. Relation of clinical culture method to T-cell memory status and efficacy in xenograft models of adoptive immunotherapy. Cytotherapy 2014;16:619–30.
46. Porter DL, Hwang WT, Frey NV, Lacey SF, Shaw PA, Loren AW, et al. Chimeric antigen receptor T cells persist and induce sustained remissions in relapsed refractory chronic lymphocytic leukemia. Sci Transl Med 2015;7:303ra139.
47. Levine BL, Cotte J, Small CC, Carroll RG, Riley JL, Bernstein WB, et al. Large-scale production of CD4+ T cells from HIV-1-infected donors after CD3/CD28 costimulation. J Hematother 1998;7:437–48.
48. Boise LH, Minn AJ, Noel PJ, June CH, Accavitti MA, Lindsten T, et al. CD28 costimulation can promote T cell survival by enhancing the expression of Bcl-xL. Immunity 1995;3:87–98.
49. Frauwirth KA, Riley JL, Harris MH, Parry RV, Rathmell JC, Plas DR, et al. The CD28 signaling pathway regulates glucose metabolism. Immunity 2002;16:769–77.
50. Weng NP, Levine BL, June CH, Hodes RJ. Regulated expression of telomerase activity in human T lymphocyte development and activation. J Exp Med 1996;183:2471–9.
51. Janetzki S, Britten CM, Kalos M, Levitsky HI, Maecker HT, Melief CJ, et al. "MIATA"-minimal information about T cell assays. Immunity 2009;31:527–8.
52. R Developmental Core Team. R: a language and environment for statistical computing. Vienna, Austria: R: Foundation for Statistical Computing; 2010.
53. McCormack E, Adams KJ, Hassan NJ, Kotian A, Lissin NM, Sami M, et al. Bi-specific TCR-anti CD3 redirected T-cell targeting of NY-ESO-1- and LAGE-1-positive tumors. Cancer Immunol Immunother 2013;62:773–85.
54. Cameron BJ, Gerry AB, Dukes J, Harper JV, Kannan V, Bianchi FC, et al. Identification of a Titin-derived HLA-A1-presented peptide as a cross-reactive target for engineered MAGE A3-directed T cells. Sci Transl Med 2013;5:197ra03.